

Diffusive versus displacive contact plasticity of nanoscale asperities: Temperature- and velocity-dependent strongest size

Wei Guo,[†] Zhao Wang,^{*,†} and Ju Li^{*,‡}

Frontier Institute of Science and Technology, and State Key Laboratory for Mechanical Behavior of Materials, Xi'an Jiaotong University, 710054, Xi'an, P. R. China., and Department of Nuclear Science and Engineering and Department of Materials Science and Engineering, Massachusetts Institute of Technology, Cambridge, Massachusetts 02139, USA

E-mail: wzzhao@yahoo.fr; liju@mit.edu

Abstract

We predict a strongest size for the contact strength when asperity radii of curvature decrease below ten nanometers. The reason for such strongest size is found to be correlated with the competition between the dislocation plasticity and surface diffusional plasticity. The essential role of temperature is calculated and illustrated in a comprehensive asperity size-strength-temperature map taking into account the effect of contact velocity. Such a map should be essential for various phenomena related to nanoscale contacts such as nanowire cold welding, self-assembly of nanoparticles and adhesive nano-pillar arrays, as well as the electrical, thermal and mechanical properties of macroscopic interfaces.

^{*}To whom correspondence should be addressed

[†]Frontier Institute of Science and Technology, and State Key Laboratory for Mechanical Behavior of Materials, Xi'an Jiaotong University, 710054, Xi'an, P. R. China.

[‡]Department of Nuclear Science and Engineering and Department of Materials Science and Engineering, Massachusetts Institute of Technology, Cambridge, Massachusetts 02139, USA

keywords: material strength, dislocation plasticity, surface diffusion, sub-10nm, Zener-Hollomon scaling

When two macroscopic solids touch, the atomistic realities of their nanoscale contacts are hidden from easy view, but they actually control how heat, electrical charge and forces are transferred across the rough interface.¹ The true contact area A_{true} , defined by atoms of the two bodies that truly interact atomistically (within certain interatomic force/distance cutoffs), is usually much smaller than the nominal macroscopic contact area A . A_{true}/A usually decreases with increasing surface roughness of the two bodies, and increases with externally applied pressure $P_{\text{ext}} \equiv -F_{\text{ext}}/A$. Recently, Pastewka and Robbins showed numerically using linear elasticity and half-space Green's function how A_{true}/A depends on P_{ext} (e.g. linearly) for two self-affine random surfaces, statistically self-similar within profile wavelengths $[\lambda_s, \lambda_L]$.² They found that when the solids are elastically compliant enough, the ratio between A_{true}/A and P_{ext} diverges due to microscopic adhesion, signifying a “non-sticky”-to-“sticky” transition of the macro-contact.

While Pastewka and Robbins' results are revealing, the assumptions of linear elasticity, especially at the lower wavelength cutoff λ_s “of order nanometers”,² could be limiting. This is because plasticity by dislocation motion and/or diffusion can occur, certainly at high enough P_{ext} , but may also occur at $P_{\text{ext}} = 0$, as we show below. One may also ask what could be a physical basis for the λ_s cutoff in solving elasticity problems - is this assumed initial condition reflecting prior history, with surface diffusional plasticity³ that tends to smooth out profile roughnesses finer than λ_s ? Incidentally, for nanostructures, Jiang *et al.*,⁴ and Guisbiers and Buchaillot⁵ have proposed size-dependent effective diffusivity

$$D(T, R) = D_{0\infty} \exp \left[-\frac{CT_{\text{m}\infty}}{k_{\text{B}}T} \left(1 - \frac{\tilde{\alpha}}{2R} \right) \right], \quad (1)$$

affecting nanoscale creep, that accompanies the well-established melting-point reduction:^{6,7}

$$T_{\text{m}}(R) = T_{\text{m}\infty} \left(1 - \frac{\alpha}{2R} \right), \quad (2)$$

where R is the radius of curvature of the nano-asperity, $T_{\text{m}\infty}$ is the bulk thermodynamic melting point, k_{B} is the Boltzmann constant, and $C, \alpha, \tilde{\alpha}, D_{0\infty}$ are temperature- and size-independent positive constants. Such “exponentially accelerated” small-size diffusive kinetics Eq.(??) seem to have some experimental support.^{8,9} While the physical basis for Eq.(??) is not as well-understood as Eq.(??), one notes that in the $R < 10\text{nm}$, and lower-homologous-temperature deformation regime that we are mostly interested in, the effective diffusivity $D(T, R)$ is dominated by the surface diffusion contribution. The activation energy Q_{S} of surface diffusion mathematically could have a leading-order correction proportional to $1/R$ in an asymptotic expansion with respect to curvature, that physically could be due to, for example, elasticity effect of the saddle-point configuration of diffusion, or the ratio of atoms near surface crystallographic facet-facet intersections (“surface defects”) among all surface atoms. In other words, the curvature effect on surface diffusion may be explained by the curvature-dependent concentration and mobility of “surface defects”. Surface diffusion could be the key for understanding λ_{s} . Recently, it was demonstrated experimentally that under an external load, or a capillarity-generated Young-Laplace pressure, plasticity by surface diffusion can indeed happen at sub-10nm lengthscale at room temperature.^{10,11}

With the above motivation, it is critical to understand the characteristics of plasticity for nanoscale asperities. Many experiments have shown that individual nano-structures can sustain close to their ideal strength¹² due to dislocation starvation. The “smaller is stronger” trend provides a strategy for increasing the material strength by nanostructuring. However when R goes down to even smaller, surface diffusion could cause dramatic softening and “smaller is much weaker”.¹³ Here we look into this issue of diffusive versus displacive contact plasticity by atomistic simulations, using the classical molecular dynamics (MD) simulator LAMMPS.¹⁴ As shown in the inset of Fig.1, in our simulations, two identical metal cylinders are moved towards each other. An embedded atom method potential¹⁵ was used to describe the atomistic interaction of Al, which is chosen because of its elastic isotropy that simplifies the analysis. We have applied displacement control $-2\Delta x(t)$ between the two rigid outer boundaries in our simulations. To contrast the outcome of different-size nano-asperities, we define total strain as $\varepsilon \equiv \Delta x(t)/R$. The stress is defined by the

engineering stress convention $\sigma_{\text{engineering}} \equiv F/A$, where F is the computed total force sustained in one of the rigid outer boundaries, and $A \equiv \pi(2R)L$ is the initial projected cross-sectional area of the cylinder, which is a “nominal” contact area in this simulation. In this paper, the “strength” of contact is defined as the time-average of $\sigma_{\text{engineering}}$ in the strain range 0.08 – 0.2 during loading, so it should be interpreted as plastic “flow strength”, and not the initiation or yield strength (see Supporting Information). R is varied from 1 to 50nm and the strain rate $\dot{\epsilon}$ is about 10^8 - 10^9 /s. MD simulations were performed using a Nosé-Hoover thermostat, and the systems were relaxed for 2ps at each load step of 0.1\AA . We note that the strain rate range 10^8 - 10^9 /s in our simulations does not induce significant difference in the final contact strengths reported.

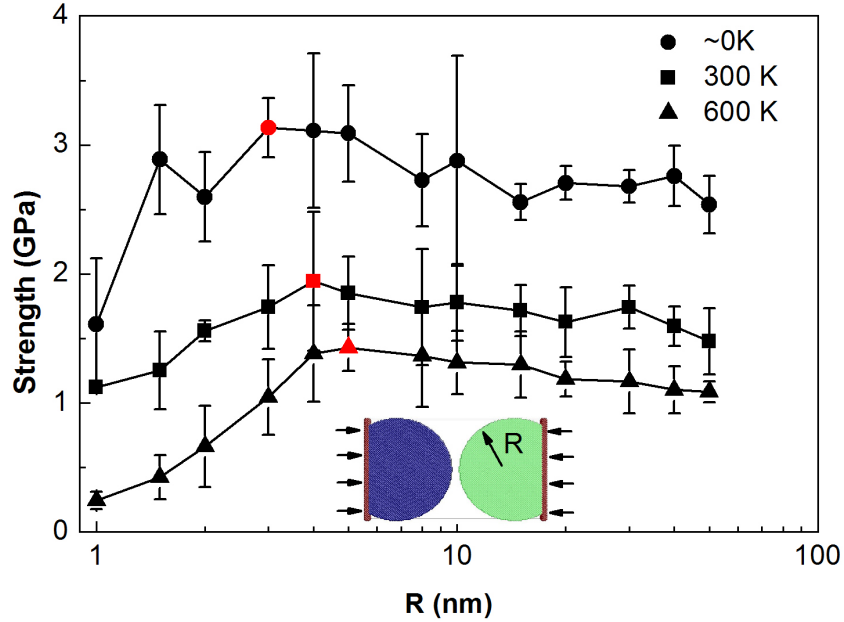


Figure 1: Contact strength as a function of the asperity radius R at different temperatures. The peak values corresponding to the strongest size are marked with red symbols. Error bars are based on the deviation of difference in three crystal orientations. Note that the strength is averaged over three crystal orientations ([100] vs. [100], [100] vs. [110], and [100] vs. [16 5 0]) with respect to the two face-centered-cubic crystals.

The size-strength relationship of our cylindrical contacts at $T = 0\text{K}$, 300K and 600K are plotted in Fig.1. It clearly shows that there exists a strongest size for the contact strength, below which the “smaller is stronger” trend no longer holds. The sharp decrease in strength when the contact

size goes down to sub-10-nm scale contradicts with the lattice dislocation-mediated deformation mechanism,^{16,17} and suggests that the strongest size is in a deformation mechanism transition zone. In our simulated samples, the critical sizes range from 5 to 10nm. In this size range, the difference between crystal and liquid surface energies causes the crystal melting point T_m to decrease as described by Eq.(??), and this effect is particularly significant in the case of $R < 10\text{nm}$.⁷ Thus, it can be expected that the surface atom diffusion may become important for the strongest size, especially when the nano-asperity is under a high load.

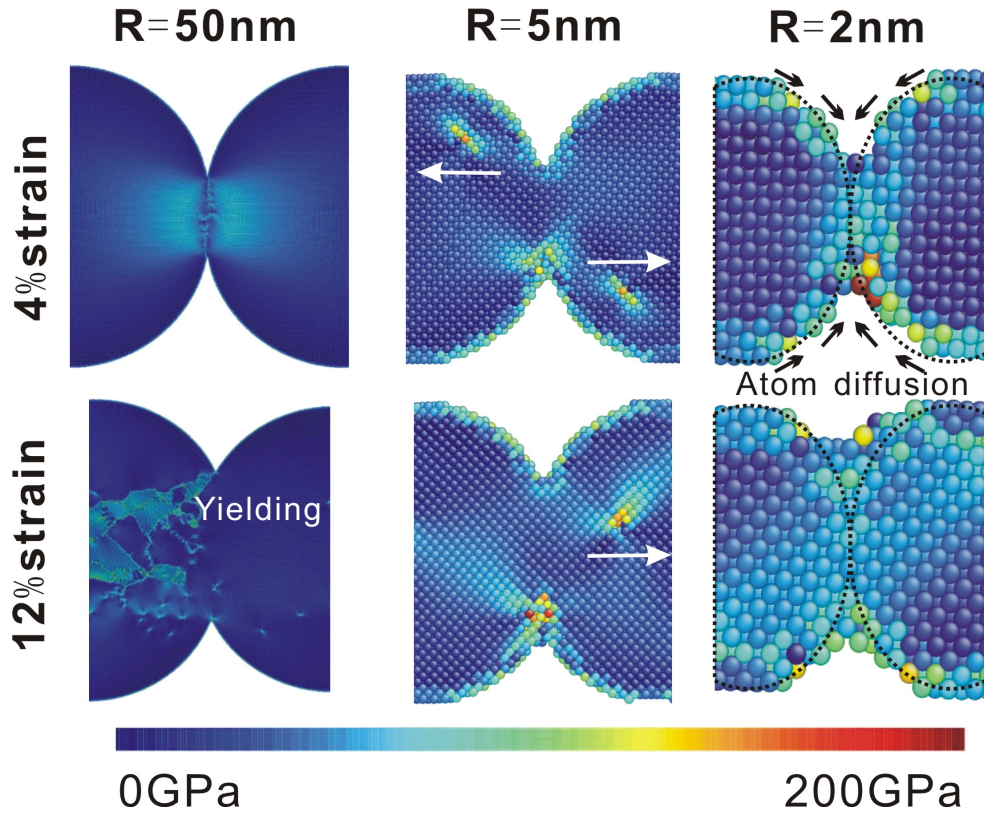


Figure 2: Snapshots of simulated room-temperature contacts of three different sizes at two different applied strain levels. The color of atoms represents the Von-Mises stress distribution. The arrows in the middle panel show the direction of dislocation displacement during loading. The arrows in the right panel show the direction of atomistic diffusion flow.

We have performed detailed analyses of the atomistic configurations and stress distributions in the simulated samples, as shown in Fig.2. A classical Hertzian stress pattern is found beneath the interface of the largest contact ($R = 50\text{nm}$) at 4% strain, and the system started to deform plastically before 12% strain. In a smaller contact ($R = 5\text{nm}$), a pair of dislocations is found to

form beneath the interface, and move to interior following increasing compressive load. After the dislocation activity, a relaxed and more homogenously distributed elastic stress results in the contacting bodies. When R decreases further down to 2nm, we visually found that the surface atoms diffuse significantly even at room temperature, in agreement with first-principles calculations.¹⁸ The atoms inside remain highly crystalline while the surface atoms diffuse to the neck region. Similar room temperature ‘liquid-like’ deformation behaviors were observed in experiments on Ag nanoparticles of about 10nm diameter,¹⁰ as well as the cold welding of Au nanowires (3 to 10nm diameter).¹⁹

To quantify diffusion in small samples under load, we apply the “deformation-diffusion” decomposition,^{20–22}

$$D_i^2 = \frac{1}{N_i} \min_{\mathbf{J}_i} \sum_{j \in N_i} | \mathbf{d}_{ji}^0 \mathbf{J}_i - \mathbf{d}_{ji} |^2, \quad (3)$$

where i, j index atoms, D_i^2 is a measure of magnitude of non-affine motion of atoms around i ; $j \in N_i$ are i ’s initial neighbors at the reference configuration, \mathbf{d}_{ji}^0 is the distance vector between atom j and i at the reference configuration, and \mathbf{d}_{ji} is the current distance vector. The local deformation gradient \mathbf{J}_i is numerically optimized to minimize D_i^2 . On the right-hand side, $\mathbf{d}_{ji}^0 \mathbf{J}_i$ stands for the displacive deformation, while $\mathbf{d}_{ji}^0 \mathbf{J}_i - \mathbf{d}_{ji}$ refers to the contribution of the non-affine, or diffusional part of the displacement.²⁰ When the contacting bodies were compressed to deformed plastically, we can see the mean D^2 fluctuates as that shown in Fig.3(a) due to the dislocation plasticity and structure collapse. It is shown that D^2 for $R = 1.5\text{nm}$ contact is the largest indicating a clearly enhanced atom diffusion. We borrow the threshold value from Lindemann criterion,²³ which was used to predict the melting point of surface confined materials, to qualitatively compare the extent of diffusion during loading. For simplicity we label an atom as diffusive when its $\sqrt{D_i^2}$ exceeds the 10% of the nearest neighbor distance. Fig.3(b) shows that a smaller contact contains a higher ratio of diffusive atoms, an observation consistent with the nanowire and nanoparticle experiments.^{5,23,24} In our $R = 2\text{nm}$ sample, the surface diffusion results in lower plastic flow stress and better adhesion. Even though diffusion is clearly accelerated by the atomic random thermal motion when the temperature increases,¹⁸ we can also observe stress-induced surface diffusion

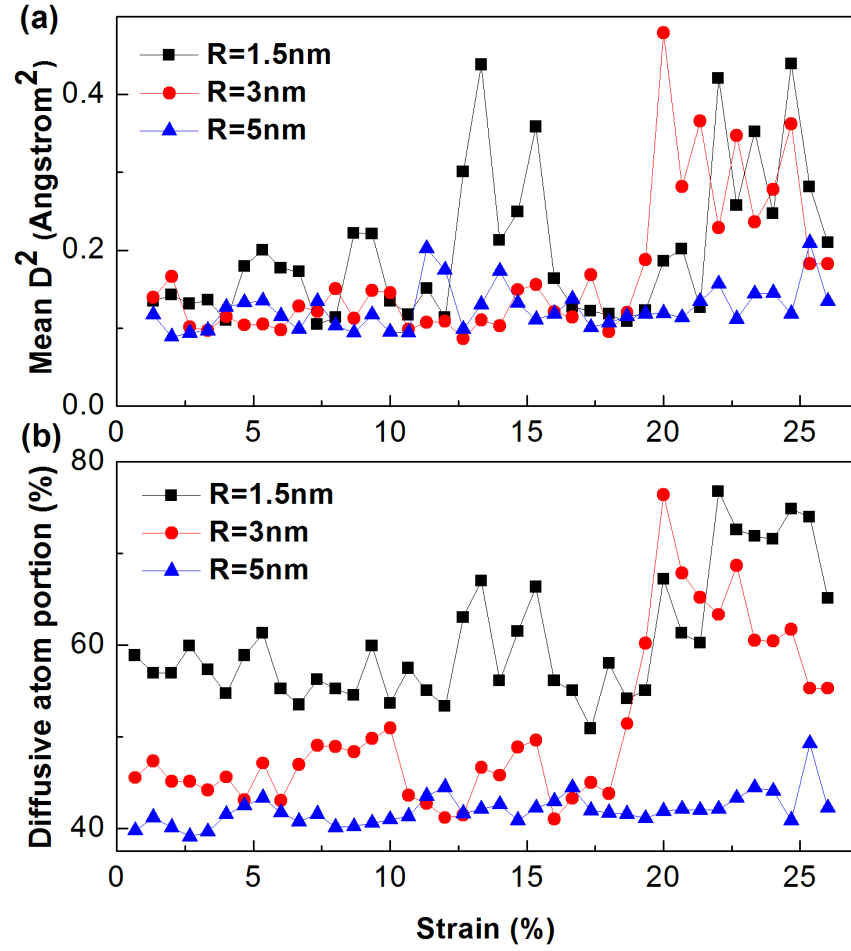


Figure 3: (a) Mean D^2 as a function of the strain in three contacts of different curvature radii. (b) Diffusive atom ratios as a function of the strain.

even at $T \rightarrow 0\text{K}$ (see our energy minimization simulation results in Supporting Information). It was suggested that this type of diffusion can be not only thermally-activated but also driven by externally applied stress²² and/or surface tension.^{11,25}

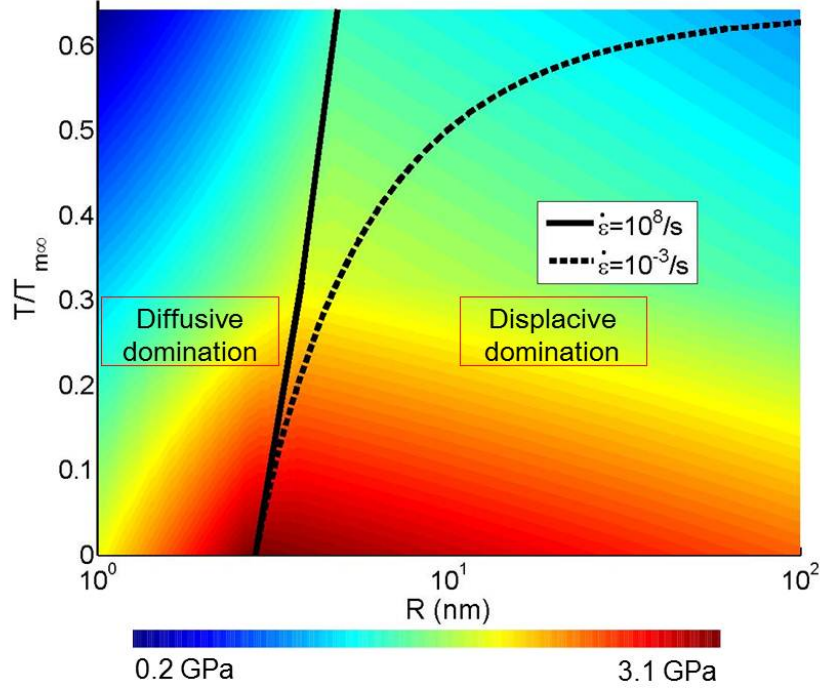


Figure 4: Contact strength mechanism map as a function of the radius of curvature (R) and homologous temperature ($T/T_{m\infty}$). The color range represents the strength values. The highest contact asperity strength computed with MD at $\dot{\epsilon} = 10^8/\text{s}$ is outlined by the solid curve. The dashed curve represents the ideal contact strength under an ordinary experimental strain rate.

The results above showed that the contact becomes “smaller is weaker” when the surface atom diffusion dominates. Based on our simulation data, we obtain a comprehensive contact size-strength-temperature map in Fig.4, illustrating the competition between the displacive and diffusion mechanisms. We find the strongest size R_c and homologous temperature $T/T_{m\infty}$ from simulations can be well-fitted as follows,

$$R_c = A \frac{T}{T_{m\infty}} + B. \quad (4)$$

We obtain $A = 3.1\text{nm}$ and $B = 2.8\text{nm}$ by fitting to our MD simulation data. However, this result

should not be directly applicable to laboratory experiments since the strain rate of the MD simulations could be many orders of magnitude higher. To overcome this limitation, we use an empirical velocity-modified temperature approach²⁶ based on the Zener-Hollomon parameter that bridges the strain rate and the temperature. This approach considers that increasing the strain rate has the similar effect as decreasing the temperature upon the stress-strain relation.²⁷ This semi-empirical relation bridges the temperature and strain rate as:

$$T_{\text{exp}} = T_{\text{MD}} \left(1 - \frac{k_B T_{\text{exp}}}{Q_S} \ln \frac{\dot{\epsilon}_{\text{MD}}}{\dot{\epsilon}_{\text{exp}}} \right), \quad (5)$$

where Q_S is an activation energy, $\dot{\epsilon}_{\text{MD}}$ is the simulation strain rate, T_{exp} is the experimental temperature and $\dot{\epsilon}_{\text{exp}}$ is the experimental strain rate. The Zener-Hollomon corrected strongest size can be derived when we combine Eqs.?? and ?? to write

$$R_c = \frac{T_{\text{exp}}}{T_{\text{m}\infty}} \left(\frac{A}{1 - \frac{k_B T_{\text{exp}}}{Q_S} \ln \left(\frac{\dot{\epsilon}_{\text{MD}}}{\dot{\epsilon}_{\text{exp}}} \right)} \right) + B. \quad (6)$$

We assume that $\dot{\epsilon}_{\text{exp}} = 10^{-3}/\text{s}$ as a typical laboratory experiment strain rate, and $Q_S = 126\text{kJ/mol} = 1.3\text{eV}$ for the aluminium system studied here,²⁸ which should be an upper bound for processes controlled by surface diffusion (and therefore gives the most sensitive strain-rate dependence). The predicted temperature-size effects at $\dot{\epsilon}_{\text{exp}} = 10^{-3}/\text{s}$ is shown by the dashed curve in Fig. 4. The sub-10-nm Au tips²⁹ and Ag particles¹⁰ at homologous temperature $T_{\text{exp}}/T_{\text{m}\infty}$ of 0.22 and 0.24 are then in the diffusion-dominated regime, which are in agreement with the experimental observations.^{10,29}

Bridging the gap between nanoscale contacts and the electrical, thermal and mechanical properties of rough macroscopic interfaces^{2,30–32} must require accurate information about the size-dependent plasticity. From Fig.1, it can be seen that the strength drops precipitously¹³ when the asperity size goes below R_c . The plastic deformation strength, which was often considered a constant, is clearly a function of the asperity size. Moreover, the correlation between the critical size and temperature/strain rate provides some physical basis for λ_s , and also a criterion to judge

whether the asperity in contact is in the diffusion-controlled regime (Fig.4), which if so is expected to bond more strongly. Such criterion may be applied to material cold welding^{1,19} and self assembly,³³ and for physics-based modeling of the electrical, thermal and mechanical properties of contacts.

Acknowledgement

This work is supported by a grant-in-aid of 985 Project from Xi'an Jiaotong University, the National Natural Science Foundation of China (Grant No. 11204228) and the National Basic Research Program of China (2012CB619402 and 2014CB644003). JL acknowledges support by NSF DMR-1410636 and DMR-1120901.

Supporting Information Available

Surface atom diffusion to contact necking region, crystal orientation combination dependence of the contact strength, Stress-strain data for explaining the strength measure. These materials are available free of charge via the Internet at <http://pubs.acs.org>.

References

- (1) G. S. Ferguson, M. K. Chaudhury, G. B. Sigal, and G. M. Whitesides, *Science* **253**, 776 (1991).
- (2) L. Pastewka and M. O. Robbins, *Proc. Natl. Acad. Sci. U.S.A* **111**, 3298 (2014).
- (3) J. Li, *Nature Materials* **14**, 656 (2015).
- (4) Q. Jiang, S. Zhang, and J. Li, *Solid State Commun.* **130**, 581 (2004).
- (5) G. Guisbiers and L. Buchailot, *Nanotechnology* **19**, 435701 (2008).
- (6) P. Buffat and J. P. Borel, *Phys. Rev. A* **13**, 2287 (1976).

- (7) M. Zhang, M. Y. Efremov, F. Schiettekatte, E. A. Olson, A. T. Kwan, S. L. Lai, T. Wisleder, J. E. Greene, and L. H. Allen, *Phys. Rev. B* **62**, 10548 (2000).
- (8) K. Dick, T. Dhanasekaran, Z. Y. Zhang, and D. Meisel, *J. Am. Chem. Soc.* **124**, 2312 (2002).
- (9) T. Shibata, B. A. Bunker, Z. Y. Zhang, D. Meisel, C. F. Vardeman, and J. D. Gezelter, *J. Am. Chem. Soc.* **124**, 11989 (2002).
- (10) J. Sun, L. He, Y.-C. Lo, T. Xu, H. Bi, L. Sun, Z. Zhang, S. X. Mao, and J. Li, *Nature Mater.* **13**, 1007 (2014).
- (11) D.-G. Xie, Z.-J. Wang, J. Sun, J. Li, E. Ma, and Z.-W. Shan, *Nature Mater.* **14**, 899-903 (2015).
- (12) T. Zhu and J. Li, *Prog. Mater. Sci.* **55**, 710 (2010).
- (13) L. Tian, J. Li, J. Sun, E. Ma, and Z.-W. Shan, *Sci. Rep.* **3**, 2113 (2013).
- (14) S. Plimpton, *J. Comput. Phys.* **117**, 1 (1995).
- (15) R. Zope and Y. Mishin, *Phys. Rev. B* **68**, 024102 (2003).
- (16) J. R. Greer, W. C. Oliver, and W. D. Nix, *Acta Mater.* **53**, 1821 (2005).
- (17) T. Zhu, J. Li, A. Samanta, A. Leach, and K. Gall, *Phys. Rev. Lett.* **100**, 25502 (2008).
- (18) M. R. Sørensen, K. W. Jacobsen, and H. Jónsson, *Phys. Rev. Lett.* **77**, 5067 (1996).
- (19) Y. Lu, J. Huang, C. Wang, S. Sun, and J. Lou, *Nature Nanotech.* **5**, 218 (2010).
- (20) C.-C. Wang, Y.-W. Mao, Z.-W. Shan, M. Dao, J. Li, J. Sun, E. Ma, and S. Suresh, *Proc. Natl. Acad. Sci. U.S.A* **110**, 19725 (2013).
- (21) M. Falk and J. Langer, *Phys. Rev. E* **57**, 7192 (1998).
- (22) W. Li, J. M. Rieser, A. J. Liu, D. J. Durian, and J. Li, *Phys. Rev. E* **91**, 062212 (2015).

- (23) Q. Mei and K. Lu, Prog. Mater. Sci. **52**, 1175 (2007).
- (24) O. Gülseren, F. Ercolessi, and E. Tosatti, Phys. Rev. B **51**, 7377 (1995).
- (25) K. Zhang, J. Weertman, and J. Eastman, Appl. Phys. Lett. **87**, 061921 (2005).
- (26) C. MacGregor and J. Fisher, J. Appl. Mech. **12**, A217 (1945).
- (27) C. Zener and J. Hollomon, J. Appl. Phys. **15**, 22 (1944).
- (28) S. Medina and C. Hernandez, Acta Mater. **44** (1996).
- (29) D. R. Strachan, D. E. Smith, M. D. Fischbein, D. E. Johnston, B. S. Guiton, M. Drndic, D. A. Bonnell, and A. T. Johnson, Nano Lett. **6**, 441 (2006).
- (30) J. Greenwood and J. Williamson, Proc. R. Soc. A **295**, 300 (1966).
- (31) B. N. J. Persson, Surf. Sci. Rep. **61**, 201 (2006).
- (32) S. Akarapu, T. Sharp, and M. O. Robbins, Phys. Rev. Lett. **106**, 204301 (2011).
- (33) R. Klajn, K. J. Bishop, M. Fialkowski, M. Paszewski, C. J. Campbell, T. P. Gray, and B. A. Grzybowski, Science **316**, 261 (2007).

This material is available free of charge via the Internet at <http://pubs.acs.org/>.